

# X-VFL: A New Vertical Federated Learning Framework with Cross Completion and Decision Subspace Alignment

Qinghua Yao\*

Singapore Management University  
& University of Pennsylvania

Xiangrui Xu\*

Singapore Management University  
& Beijing Jiaotong University

Zhize Li†

Singapore Management University

August 7, 2025

## Abstract

Vertical Federated Learning (VFL) enables collaborative learning by integrating disjoint feature subsets from multiple clients/parties. However, VFL typically faces two key challenges: i) the requirement for perfectly aligned data samples across all clients (missing features are not allowed); ii) the requirement for joint collaborative inference/prediction involving all clients (it does not support locally independent inference on a single client). To address these challenges, we propose X-VFL, a new VFL framework designed to deal with the non-aligned data samples with (partially) missing features and to support locally independent inference of new data samples for each client. In particular, we design two novel modules in X-VFL: *Cross Completion* (XCom) and *Decision Subspace Alignment* (DS-Align). XCom can complete/reconstruct missing features for non-aligned data samples by leveraging information from other clients. DS-Align aligns local features with completed and global features across all clients within the decision subspace, thus enabling locally independent inference at each client. Moreover, we provide convergence theorems for different algorithms used in training X-VFL, showing an  $O(1/\sqrt{T})$  convergence rate for SGD-type algorithms and an  $O(1/T)$  rate for PAGE-type algorithms, where  $T$  denotes the number of training update steps. Extensive experiments on real-world datasets demonstrate that X-VFL significantly outperforms existing methods, e.g., achieving a 15% improvement in accuracy on the image CIFAR-10 dataset and a 43% improvement on the medical MIMIC-III dataset. These results validate the practical effectiveness and superiority of X-VFL, particularly in scenarios involving partially missing features and locally independent inference.

## 1 Introduction

Federated Learning (FL) is a collaboratively learning framework where multiple clients/parties jointly train a machine learning model under the coordination of a central server without sharing their raw data (McMahan et al., 2017; Kairouz et al., 2021). Based on the partitioning of sample

---

\*Equal contribution. The work of Qinghua Yao and Xiangrui Xu was conducted during their time as Visiting Research Students in Zhize Li's group at SMU.

†Corresponding author ([zhizeli@smu.edu.sg](mailto:zhizeli@smu.edu.sg)).

and feature spaces, FL can be categorized into Horizontal FL (HFL) and Vertical FL (VFL) (Yang et al., 2019; Kairouz et al., 2021; Liu et al., 2024). In HFL, different clients typically hold different local datasets that share the same feature space, whereas in VFL, all clients use the same set of data samples but each holds a different subset of features.

In this paper, we focus on VFL, which is particularly useful in domains such as finance, healthcare, and e-commerce, where participating clients/parties often possess complementary feature sets (Joshi et al., 2022; Liu et al., 2024). For a VFL framework with  $k$  clients, each client  $i$  contains a subset of features, denoted as  $\mathbf{X}_i = (\mathbf{X}_i^{al}, \mathbf{X}_i^{nl})$ . Here,  $\mathbf{X}_i^{al}$  represents aligned samples, where all clients have full local feature sets for these samples without any missing features.  $\mathbf{X}_i^{nl}$  denotes non-aligned samples, where at least one client has (partially) missing features. Fig. 1 illustrates this data partition in VFL with two clients  $k = 2$ .

While VFL represents a promising framework by integrating disjoint local feature sets from multiple clients, its practical deployment is often hindered by two major limitations. First, both training and inference processes in VFL depend on the complete alignment of data samples across all clients (Castiglia et al., 2022a; Kang et al., 2022), i.e., only use the aligned samples  $\mathbf{X}^{al}$ . This requirement significantly limits the volume of usable data, thereby affecting both the model accuracy and the scalability of the model. Second, the inference phase necessitates collaboration with all clients to complete the inference process, leading to significant communication overhead and making real-time or locally independent inference impractical (Li et al., 2022b; Ren et al., 2022). These limitations highlight an urgent need to develop a VFL framework to facilitate independent inferences and enable the efficient exploitation of non-aligned data samples (i.e.,  $\mathbf{X}^{nl}$ ) during both training and inference processes.

In this paper, we propose X-VFL, a novel VFL framework that exploits the non-aligned data samples with missing features and supports locally independent inference of new data samples for each client. Particularly, we design two key modules in X-VFL: *Cross Completion* (XCom) and *Decision Subspace Alignment* (DS-Align). The XCom module is developed to establish cross-complementary dependencies among disjoint local features contributed by different clients. Leveraging these relationships, local clients can complete their missing features through XCom, thereby effectively increasing the volume of data available for training and inference. The DS-Align module is designed to align the features across all clients within the decision subspace to support locally independent inference for each client, while maintaining performance comparable to collaborative inferences involving all clients.

As illustrated in the attention heatmap (Fig. 2), the image is partitioned between two clients (left and right). In the “Single” setting, the left-side client entirely lacks its local features. Consequently, the model relies solely on the right-side client’s features resulting in a relatively low confidence score of 0.728 for the

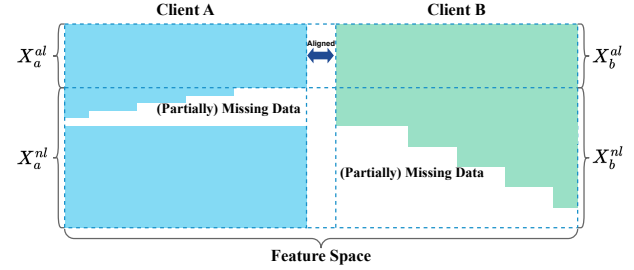


Figure 1: Dataset partition in VFL with  $k = 2$ .

Figure 1: Dataset partition in VFL with  $k = 2$ .

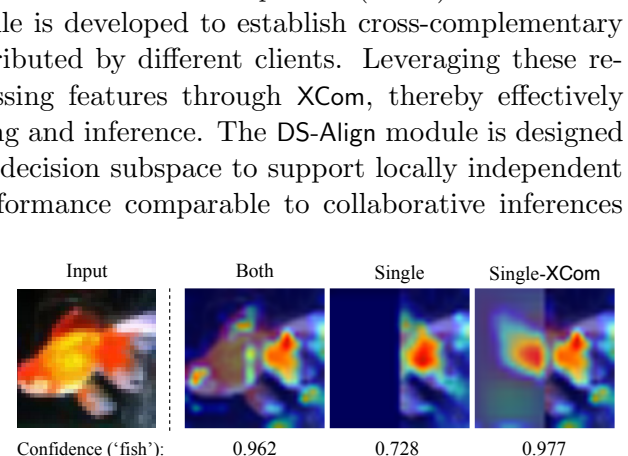


Figure 2: Effect of XCom.

“fish” class. However, with the integration of our XCom (“Single-XCom”), the missing features in the left-side client are completed using the information from the right-side client through XCom. As a result, “Single-XCom” significantly improves the confidence score to 0.977. Moreover, it even slightly exceeds the 0.962 confidence score obtained when using the full joint features (“Both”), showing that XCom may also help denoise the original data and enhance inference accuracy. These results highlight the effectiveness of XCom in reconstructing missing features and improving model performance.

The proposed DS-Align module enhances X-VFL by aligning local individual features with the completed and joint features across all clients within the decision subspace. This alignment enables locally independent inference even in the presence of missing features. As shown in Fig. 3, the “Vanilla” setting (Fig. 3a) results in a poorly defined decision boundary, leading to overlapping regions and misclassifications. In contrast, our “DS-Align” setting (Fig. 3b) yields a much clearer decision boundary, ensuring better separation between classes. This confirms the effectiveness of DS-Align in inference under our X-VFL framework.

## 1.1 Our Contributions

We would like to highlight the following contributions:

- We propose X-VFL, a novel VFL framework designed to handle the non-aligned data samples with (partially) missing features and to support locally independent inference for new data samples at each client. More importantly, our X-VFL introduces two key modules: Cross Completion (XCom) and Decision Subspace Alignment (DS-Align), which significantly enhance the ability of VFL to address more complex and practical scenarios.
- To the best of our knowledge, we are the first to introduce a practical setting with *partially* missing features in VFL, where a client may retain some local features rather than fully missing all local features for non-aligned data samples. For example, consider a non-aligned data sample  $X$  with  $m$  features evenly partitioned between two clients, each holding  $\frac{m}{2}$  features. Previous studies have only considered the fully missing setting, where one client lacks all  $\frac{m}{2}$  of its local features. However, we introduce the notion *missing rate*, denoted as  $R_{\text{miss}}$ , where a client may miss  $R_{\text{miss}} \cdot \frac{m}{2}$  of its local features. In particular, the missing rate  $R_{\text{miss}} = 1$  recovers the fully missing case. Given the ubiquity of partially missing features in real-world datasets, addressing this more general and realistic setting is essential for enhancing the practical applicability of VFL.
- Moreover, we provide theoretical convergence theorems for the algorithms used in training X-VFL, showing an  $O(1/\sqrt{T})$  convergence rate for SGD-type algorithms and an  $O(1/T)$  rate for PAGE-type algorithms, where  $T$  denotes the number of training update steps (see Theorems 1 and 2 in Section 3).
- Finally, we conduct extensive experiments on real-world datasets to demonstrate that X-VFL significantly outperforms existing VFL methods, e.g., achieving a 15% improvement

in accuracy on CIFAR-10 and a 43% improvement on the medical dataset MIMIC-III (see Section 4). The experiments validate the practical effectiveness and superiority of X-VFL in VFL, particularly in practical scenarios involving partially missing features and locally independent inference.

## 1.2 Related Work

Vertical Federated Learning (VFL) enables distributed learning on vertically partitioned datasets, where clients hold disjoint feature subsets of the same dataset samples (Liu et al., 2024). A substantial body of work has focused on reducing communication overhead, which is critical for improving the scalability and practicality of VFL, making it a promising research direction (Castiglia et al., 2022b; Fu et al., 2022; Huang et al., 2022).

In addition, several studies have explored Split Neural Network (SplitNN)-based VFL architectures to facilitate multi-client collaboration without direct data sharing (Vepakomma et al., 2018; Thapa et al., 2022). In these architectures, each client trains a segment of a neural network up to a predefined cut layer. The outputs at the cut layer from each client are transmitted to a central server, which holds the class labels and completes the forward and backward propagation. The resulting gradients are sent back to the clients to update their local models. This iterative process is repeated until convergence. During inference, predictions are collaboratively generated by all clients.

Research on SplitNN-based VFL mainly focused on enabling locally independent inference and handling non-aligned data samples (Liu et al., 2024). For instance, Ren et al. (2022) introduced a knowledge distillation framework, IAVFL, that transfers insights from joint training to local models, enabling independent inference based solely on local features. Subsequent studies extended this concept through representation-level distillation to capture inter-client feature correlations and enhance independent inference capabilities (Huang et al., 2023; Li et al., 2022a; Lin et al., 2020). However, these distillation-based methods are restricted to aligned samples, thus providing limited improvement in inference performance.

Another promising direction leverages non-aligned data to improve model performance (Li et al., 2022b; Xu et al., 2023). Recent efforts have applied self-supervised learning (SSL) techniques to enhance local model representations using non-aligned data samples (Castiglia et al., 2022a; Xu et al., 2023). By improving the representational quality of local models, SSL typically contributes to better global model performance in VFL frameworks. However, these methods still require collaboration among all clients during the inference, restricting their practical applicability. Besides, Kang et al. (2022) proposed a semi-supervised learning framework, FedCVT, that estimates the corresponding embeddings/representations for the missing features and infers the pseudo labels for the missing labels, thus increasing the amount of data embeddings available for training. Valdeira et al. (2025) proposed LASER-VFL, a VFL framework that enables training and inference with subsets of feature blocks by sharing representation models and using average aggregation with task sampling. However, it only considers the fully missing feature setting and does not support partially missing features. Moreover, it lacks the ability to complete/reconstruct missing features.

Therefore, designing a new VFL framework that supports independent inferences and enables the efficient integration and completion of non-aligned data samples with partially missing features during both training and inference is critical for advancing the practical capabilities of VFL.

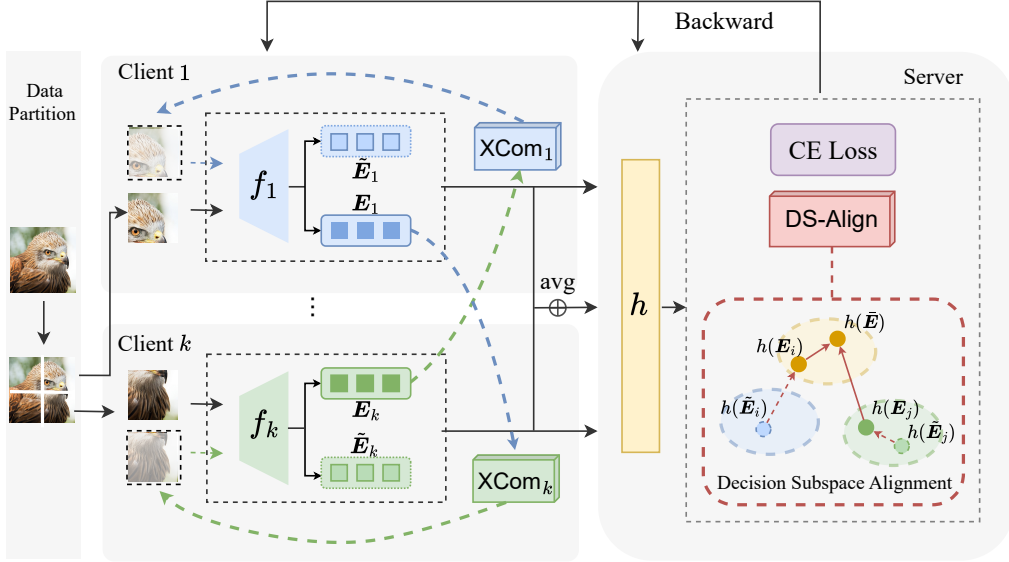


Figure 4: The framework of X-VFL.

## 2 X-VFL Framework

In this section, we introduce X-VFL, a novel framework that overcomes the limitations of conventional VFL by supporting locally independent inference and effectively handling datasets with partially missing features. In Section 2.1, we first describe the setup used in our X-VFL, which serves as the base for supporting both collaborative and independent inference under partially missing features. Then, we provide an overview of the X-VFL framework by introducing its two core components: Cross Completion (XCom) and Decision Subspace Alignment (DS-Align). Finally, we present the inference modes supported by our X-VFL in Section 2.2, which include both collaborative and independent inference while effectively handling partially missing features.

### 2.1 Framework description

As illustrated in Fig. 4, our X-VFL is built upon two key modules: Cross Completion (XCom) and Decision Subspace Alignment (DS-Align). Each client hosts a local/bottom model  $f_i$  and an XCom module. The local model  $f_i$  processes its local features to high-level embeddings/representations, denoted as  $E_i = f_i(x_i)$ , while the XCom module reconstructs missing features using embeddings received from other clients. Once the embeddings, whether derived from existing features, reconstructed features, or a combination of both, are obtained, they are either directly fed into the top model  $h$  or averaged before being used as input. The final loss is computed by combining the decision cross-entropy (CE) loss and the loss from the DS-Align module, followed by standard backpropagation.

Note that previous VFL frameworks typically aggregates the embeddings via direct concatenation:  $\mathbf{E} = [\mathbf{E}_1, \mathbf{E}_2, \dots, \mathbf{E}_k]$ , combining representations from all clients. However, our X-VFL performs aggregation via averaging  $\mathbf{E}_{\text{avg}} = \text{Avg}(\mathbf{E}_1, \mathbf{E}_2, \dots, \mathbf{E}_k)$ , and uses  $\mathbf{E}_{\text{avg}}$  as the input to the top model. This design naturally enables *independent inference*, as each local embedding  $E_i$  has the same dimensionality as  $\mathbf{E}_{\text{avg}}$ , allowing a single client to perform inference locally using its local

model  $f_i$  with the top model  $h$ . In contrast, under previous concatenation-based design, the global embedding  $\mathbf{E}$  (input to the top model  $h$ ) differs in dimensionality from individual embedding  $\mathbf{E}_i$ , thus requiring all clients to participate for inference (i.e., collaborative inference).

**Cross Completion.** The XCom module is designed to complete/reconstruct missing features for non-aligned data samples by leveraging information from other clients, thereby increasing the amount of usable training data and improving the inference performance.

To better illustrate this, we first consider a two-client setting with clients A and B (the general case with multiple  $k$  clients is deferred to Appendix D). Let  $f_a$  and  $f_b$  denote their bottom models, respectively. Their (partially) missing features can be completed using the embeddings of the other client as follows:

$$\tilde{\mathbf{X}}_a = \text{XCom}_a(\mathbf{E}_b), \quad \tilde{\mathbf{X}}_b = \text{XCom}_b(\mathbf{E}_a), \quad (1)$$

where  $\mathbf{E}_b = f_b(\mathbf{X}_b)$  and  $\mathbf{E}_a = f_a(\mathbf{X}_a)$ ,  $\text{XCom}_a$  and  $\text{XCom}_b$  are feature completers hosted by client A and client B, respectively. For the fully missing feature scenario, the completed features  $\tilde{\mathbf{X}}_a$  and  $\tilde{\mathbf{X}}_b$  are entirely adopted. For the partially missing feature scenario, only the components of  $\tilde{\mathbf{X}}_a$  and  $\tilde{\mathbf{X}}_b$  for missing features are adopted, while the remaining components should be replaced by their corresponding existing features in the original positions. The completed features  $\tilde{\mathbf{X}}_a$  and  $\tilde{\mathbf{X}}_b$  are then input into their corresponding bottom models,  $f_a$  and  $f_b$ , to generate their embeddings  $\tilde{\mathbf{E}}_a$  and  $\tilde{\mathbf{E}}_b$ , respectively.

Then, the classification decision loss is formulated as follows:

$$\begin{aligned} L_{\text{decision}} = & \ell(h(\mathbf{E}_a), y) + \ell(h(\mathbf{E}_b), y) + \ell(h(\frac{\mathbf{E}_a + \mathbf{E}_b}{2}), y) \\ & + \ell(h(\frac{\mathbf{E}_a + \tilde{\mathbf{E}}_b}{2}), y) + \ell(h(\frac{\tilde{\mathbf{E}}_a + \mathbf{E}_b}{2}), y), \end{aligned} \quad (2)$$

where  $\ell$  denotes the classification loss, e.g., cross-entropy (CE) loss.  $\ell(h(\mathbf{E}_a), y)$  and  $\ell(h(\mathbf{E}_b), y)$  ensure that the model maintains the ability to make accurate predictions based on features from a single client, thereby supporting independent inference. The term  $\ell(h(\frac{\mathbf{E}_a + \mathbf{E}_b}{2}), y)$  reinforces the model's capacity to leverage the combined features, enhancing collaborative inference performance. The terms involving reconstructed embeddings, i.e.,  $\ell(h(\frac{\mathbf{E}_a + \tilde{\mathbf{E}}_b}{2}), y)$  and  $\ell(h(\frac{\tilde{\mathbf{E}}_a + \mathbf{E}_b}{2}), y)$ , ensure that the reconstructed embeddings ( $\tilde{\mathbf{E}}_a$  or  $\tilde{\mathbf{E}}_b$ ) effectively compensate for the missing information, thus enabling robust inference in the presence of missing features. For aligned data, all terms should be activated. For non-aligned data, we consider two cases: 1) Client A has full local features while client B has (partially) missing features. In this case, the loss terms  $\ell(h(\mathbf{E}_a), y)$  and  $\ell(h(\frac{\mathbf{E}_a + \tilde{\mathbf{E}}_b}{2}), y)$  are activated; 2) The roles are reversed; client B has full local features, and client A has (partially) missing features. The activated terms are  $\ell(h(\mathbf{E}_b), y)$  and  $\ell(h(\frac{\tilde{\mathbf{E}}_a + \mathbf{E}_b}{2}), y)$ .

By explicitly leveraging reconstructed features, XCom effectively addresses the challenges of training and inference with (partially) missing features in VFL.

**Decision Subspace Alignment.** DS-Align unifies the alignment between reconstructed and existing features for aligned data, as well as between local individual features and the joint averaged features aggregated from all clients, within the decision subspace. This reinforces the effectiveness of XCom and further enhances the performance of independent inference.

To enforce consistency between reconstructed features and their corresponding existing features, ensuring accurate and reliable feature completion, DS-Align introduces the following alignment loss

within the decision subspace:

$$L_{\text{DSAlign}_1} = \ell(h(\tilde{\mathbf{E}}_a), h(\mathbf{E}_a)) + \ell(h(\tilde{\mathbf{E}}_b), h(\mathbf{E}_b)), \quad (3)$$

where  $\ell$  represents a similarity loss function, e.g., mean square error (MSE), which ensures that inference based on reconstructed embeddings aligns closely with the existing embeddings.

To enhance the performance of independent inference, DS-Align aligns local individual features and joint averaged features from all clients within the decision subspace. This alignment enables more accurate independent inference and is formulated as:

$$L_{\text{DSAlign}_2} = \ell(h(\mathbf{E}_a), h(\frac{\mathbf{E}_a + \mathbf{E}_b}{2})) + \ell(h(\mathbf{E}_b), h(\frac{\mathbf{E}_a + \mathbf{E}_b}{2})). \quad (4)$$

This dual-component approach reinforces both feature completion and independent inference, thus enhancing the overall performance and scalability of X-VFL.

Finally, by integrating XCom and DS-Align, we formulate the overall loss function for our X-VFL framework as follows:

$$L = L_{\text{decision}} + \lambda_1 L_{\text{DSAlign}_1} + \lambda_2 L_{\text{DSAlign}_2}. \quad (5)$$

Here,  $L_{\text{decision}}$  (see Eq. (2)) denotes the classification decision loss for both aligned and non-aligned data samples, while  $L_{\text{DSAlign}_1}$  and  $L_{\text{DSAlign}_2}$  (see Eq. (3) and Eq. (4)) are the two loss components introduced by our DS-Align, weighted by the hyperparameters  $\lambda_1$  and  $\lambda_2$ , respectively.

## 2.2 Inference modes of X-VFL

As illustrated in Fig. 5, the X-VFL framework supports multiple inference modes to highlight the flexibility and scalability of X-VFL:

1. **Independent inference without missing features** (Fig. 5a): Each client independently generates predictions using only its local features and model, without requiring cross-client communication during inference.
2. **Independent inference with missing features** (Fig. 5b): Each client leverages its XCom module to reconstruct missing features and produce predictions independently.
3. **Collaborative inference with/without missing features** (Fig. 5c): All clients contribute their feature embeddings (obtained either from the original data or from the reconstructed data via XCom) to the central server, enabling comprehensive and robust predictions through collaborative inference.

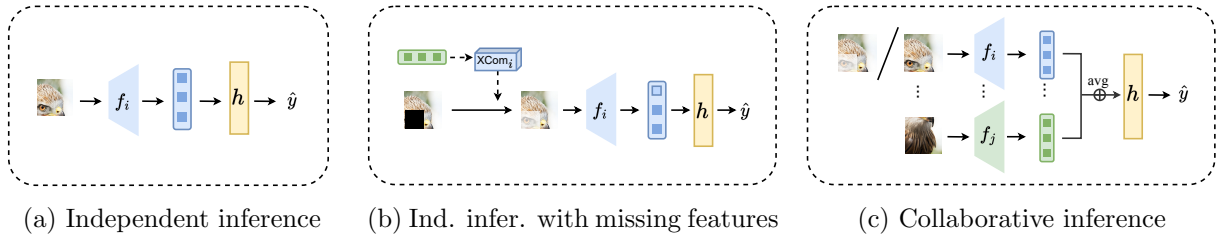


Figure 5: Different inference modes of X-VFL for independent and collaborative inference, with/without missing features.

### 3 Theoretical Results

In this section, we provide theoretical convergence theorems for our X-VFL framework which is formulated as the following optimization problem (see Eq. (5) in Section 2.1):

$$\min_{\boldsymbol{\theta}} L(\boldsymbol{\theta}) := L_{\text{decision}} + \lambda_1 L_{\text{DSAlign}_1} + \lambda_2 L_{\text{DSAlign}_2}, \quad (6)$$

where  $\boldsymbol{\theta} \in \mathbb{R}^d$  denotes the X-VFL model parameters,  $\lambda_1 \in \mathbb{R}$  and  $\lambda_2 \in \mathbb{R}$  are two hyperparameters. To present the theorems, we first introduce the necessary notation and assumptions.

#### 3.1 Notation and assumptions

Let  $\Delta_0 := L(\boldsymbol{\theta}^0) - L^*$ , where  $L^* := \min_{\boldsymbol{\theta}} L(\boldsymbol{\theta})$ . Let  $\nabla L(\boldsymbol{\theta})$  denote the gradient of function  $L$  at point  $\boldsymbol{\theta}$ ,  $\tilde{\nabla}L(\boldsymbol{\theta})$  and  $\tilde{\nabla}_b L(\boldsymbol{\theta})$  denote its stochastic gradient and minibatch stochastic gradients with size  $b$ . Let  $[n]$  denote the set  $\{1, 2, \dots, n\}$  and  $\|\cdot\|$  denote the Euclidean norm for a vector. Let  $\langle \mathbf{u}, \mathbf{v} \rangle$  denote the inner product of two vectors  $\mathbf{u}$  and  $\mathbf{v}$ . We use  $O(\cdot)$  to hide absolute constants.

In order to prove the convergence results, one usually needs the following standard smoothness assumption and stochastic gradient variance assumption (see e.g., Ghadimi et al., 2016; Fang et al., 2018; Li et al., 2021; Li and Richtárik, 2020).

**Assumption 1 (Average smoothness)** *A function  $f : \mathbb{R}^d \rightarrow \mathbb{R}$  is average  $\beta$ -smooth if*

$$\mathbb{E}[\|\tilde{\nabla}L(\boldsymbol{\theta}_1) - \tilde{\nabla}L(\boldsymbol{\theta}_2)\|^2] \leq \beta^2 \|\boldsymbol{\theta}_1 - \boldsymbol{\theta}_2\|^2, \quad \forall \boldsymbol{\theta}_1, \boldsymbol{\theta}_2 \in \mathbb{R}^d. \quad (7)$$

**Assumption 2 (Bounded variance)** *The stochastic gradient  $\tilde{\nabla}L(\boldsymbol{\theta})$  is unbaised and has bounded variance*

$$\mathbb{E}[\|\tilde{\nabla}L(\boldsymbol{\theta}) - \nabla L(\boldsymbol{\theta})\|^2] \leq \sigma^2, \quad \forall \boldsymbol{\theta} \in \mathbb{R}^d. \quad (8)$$

#### 3.2 Convergence results

Now we present the convergence theorems for training X-VFL to find a suitable target parameter  $\hat{\boldsymbol{\theta}}$ . The convergence theorems can also indicate the communication complexity and computation complexity of different algorithms (such as standard stochastic gradient descent (SGD) and the optimal variance-reduced PAGE (Li et al., 2021)) for training X-VFL.

**Theorem 1 (Convergence for SGD-type algorithms)** *Suppose that Assumptions 1 and 2 hold. For SGD-type algorithms, e.g., update  $\boldsymbol{\theta}^{t+1} = \boldsymbol{\theta}^t - \eta \tilde{\nabla}L(\boldsymbol{\theta}^t)$ , after  $T$  steps, we have  $\frac{1}{T} \sum_{t=0}^{T-1} \mathbb{E} \|\nabla L(\boldsymbol{\theta}^t)\|^2 \leq \frac{\Delta_0}{(\eta - \beta\eta^2/2)T} + \frac{\beta\eta^2\sigma^2}{2\eta - \beta\eta^2}$ . Choose learning rate  $\eta \leq \min\{\frac{2}{\beta}, \sqrt{\frac{2\Delta_0}{\beta\sigma^2 T}}\}$ , we obtain*

$$\frac{1}{T} \sum_{t=0}^{T-1} \mathbb{E} \|\nabla L(\boldsymbol{\theta}^t)\|^2 \leq O\left(\frac{1}{\sqrt{T}}\right). \quad (9)$$

This means that after  $T = O(\frac{1}{\epsilon^4})$  steps, SGD-type algorithms can find a suitable parameter  $\hat{\boldsymbol{\theta}}$  for X-VFL such that  $\mathbb{E} \|\nabla L(\hat{\boldsymbol{\theta}})\|^2 \leq \epsilon^2$ , where  $\epsilon$  denotes the convergence error.

Note that each update step requires one round of communication in X-VFL, so the total number of communication rounds is  $T = O(\frac{1}{\epsilon^4})$ . Also, each step incurs a computational cost corresponding to a stochastic gradient computation  $\tilde{\nabla}L(\boldsymbol{\theta}^t)$ .

We note that the large number of communication rounds is mainly due to the variance in stochastic gradients. Thus we also show that the optimal variance-reduced PAGE method (Li et al., 2021) can largely reduce the number of communication rounds, i.e., from  $T = O(\frac{1}{\epsilon^4})$  to  $T = O(\frac{1}{\epsilon^2})$  by a factor of  $\frac{1}{\epsilon^2}$ . A simplified PAGE update at step  $t$  is

$$\boldsymbol{\theta}^{t+1} = \boldsymbol{\theta}^t - \eta \mathbf{g}^t, \quad \text{where } \mathbf{g}^t = \begin{cases} \tilde{\nabla}_b L(\boldsymbol{\theta}^t) & \text{with probability } p \\ \mathbf{g}^{t-1} + \tilde{\nabla}_{b'} L(\boldsymbol{\theta}^t) - \tilde{\nabla}_{b'} L(\boldsymbol{\theta}^{t-1}) & \text{with probability } 1-p \end{cases}. \quad (10)$$

It uses minibatch SGD update  $\tilde{\nabla}_b L(\boldsymbol{\theta}^t)$  with probability  $p$ , and reuses the previous gradient  $\mathbf{g}^{t-1}$  with a small adjustment (lower computation cost if  $b' \ll b$ ). This update reduces the variance in stochastic gradients during training and thus significantly decreases the total number of communication rounds, i.e., by a factor of  $\frac{1}{\epsilon^2}$ .

**Theorem 2 (Convergence for PAGE-type algorithms)** *Suppose that Assumptions 1 and 2 hold. For PAGE-type algorithms, e.g., update as Eq. (10), after  $T$  steps, we have  $\frac{1}{T} \sum_{t=0}^{T-1} \mathbb{E} \|\nabla L(\boldsymbol{\theta}^t)\|^2 \leq \frac{2\Delta_0}{\eta T} + \frac{\sigma^2}{pbT} + \frac{\sigma^2}{b}$ . Choose learning rate  $\eta \leq \frac{1}{2\beta}$ , minibatch sizes  $b = \frac{2\sigma^2}{\epsilon^2}$ ,  $b' \leq \sqrt{b}$  and probability  $p = \frac{b'}{b+b'}$ , we obtain*

$$\frac{1}{T} \sum_{t=0}^{T-1} \mathbb{E} \|\nabla L(\boldsymbol{\theta}^t)\|^2 \leq O\left(\frac{1}{T}\right). \quad (11)$$

This means that after  $T = O(\frac{1}{\epsilon^2})$  steps, PAGE-type algorithms can find a suitable parameter  $\hat{\boldsymbol{\theta}}$  for X-VFL such that  $\mathbb{E} \|\nabla L(\hat{\boldsymbol{\theta}})\|^2 \leq \epsilon^2$ , where  $\epsilon$  denotes the convergence error.

Similarly, each update step requires one round of communication in X-VFL, so the total number of communication rounds is  $T = O(\frac{1}{\epsilon^2})$ . Also, each step incurs a computational cost corresponding to a minibatch stochastic gradients computation with expected size  $pb + (1-p)b' = \frac{b'b}{b+b'} + \frac{bb'}{b+b'} \leq 2b'$ .

## 4 Experiments

In this section, we present a comprehensive empirical evaluation of the proposed X-VFL framework using 6 real-world datasets (three image datasets: CIFAR-10 (Krizhevsky et al., 2009), TinyImageNet (restricted to five classes) (Deng et al., 2009), UTKFace (Zhang et al., 2017), and three tabular datasets: MIMIC-III (Johnson et al., 2016), Bank (Liang et al., 2016), and Avazu (Kang et al., 2022)). We compare our X-VFL against four methods (Vanilla Standalone, Vanilla VFL, IAVFL (Ren et al., 2022), FedCVT (Kang et al., 2022)). We conduct experiments under a variety of practical scenarios, including: varying feature missing rates within each client (see Section 4.1), varying overlap ratios of aligned data samples (see Section 4.2), and imbalanced training data across clients (see Section 4.3). More details of the experimental setup are provided in Appendix B. Additional experiments on more datasets and in the multiple clients setting are deferred to Appendix C and D, respectively.

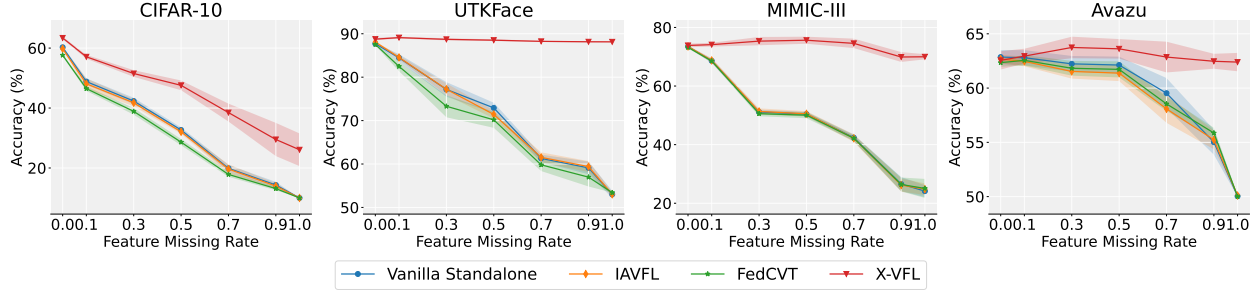


Figure 6: Performance comparison under varying feature missing rates in the independent inference mode on the CIFAR-10, UTKFace, MIMIC-III, and Avazu datasets.

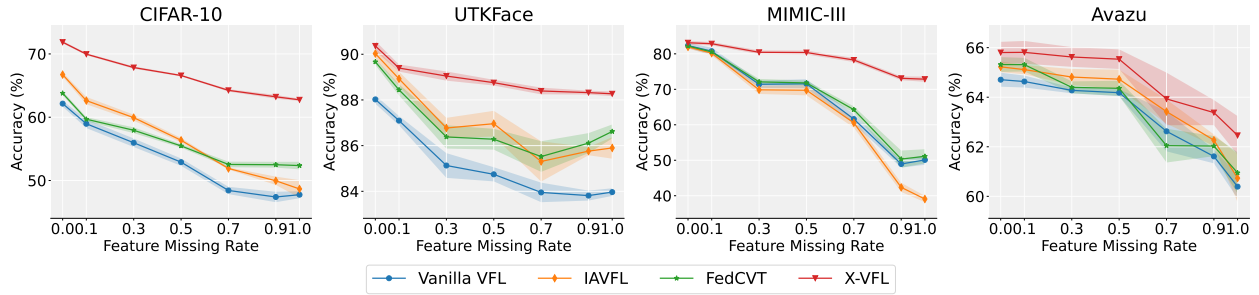


Figure 7: Performance comparison under varying feature missing rates in the collaborative inference mode on the CIFAR-10, UTKFace, MIMIC-III, and Avazu datasets.

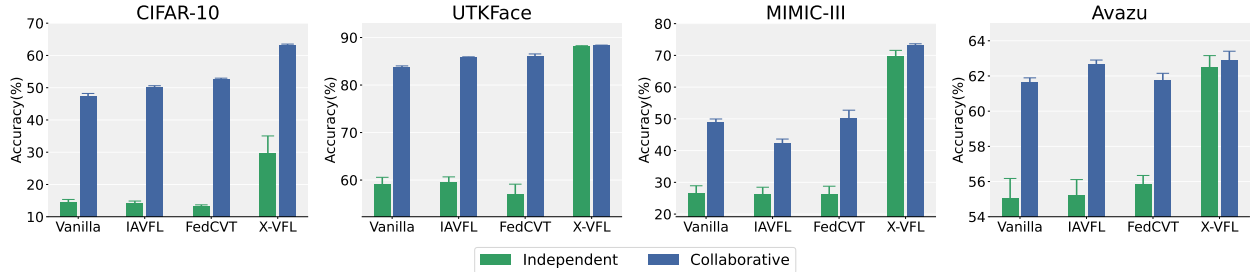


Figure 8: Performance comparison between independent and collaborative inference modes under feature missing rate  $R_{\text{miss}} = 0.9$  on the CIFAR-10, UTKFace, MIMIC-III, and Avazu datasets.

#### 4.1 Results under varying feature missing rates

The experimental results on CIFAR-10, UTKFace, MIMIC-III, and Avazu are summarized in Fig. 6 and Fig. 7, corresponding to the independent and collaborative inference modes, respectively. A comparison of performance between these two modes at a missing rate  $R_{\text{miss}} = 0.9$  is presented in Fig. 8.

As shown in Fig. 6 and Fig. 7, X-VFL consistently outperforms all methods across all datasets and feature missing rates, in both independent and collaborative modes. Moreover, the performance gap further widens as the missing rate increases. For instance, on the UTKFace dataset (in Fig. 6) with a feature missing rate  $R_{\text{miss}} = 0.9$ , the independent prediction accuracies of the three baseline

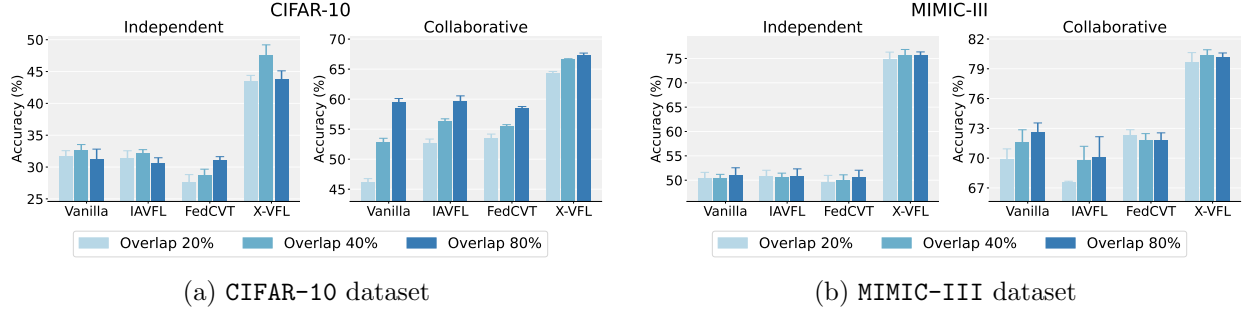


Figure 9: Performance comparison under varying overlap ratios on the CIFAR-10 and MIMIC-III datasets.

methods drop from nearly 90% (at  $R_{\text{miss}} = 0$ , i.e., no missing data) to around 60%, indicating a performance degradation of 30%. In contrast, X-VFL maintains high accuracy under the same condition, with a decrease of less than 0.5% compared to its own performance at  $R_{\text{miss}} = 0$ .

Fig. 8 highlights the advantage of X-VFL over the baseline methods by demonstrating its ability to effectively narrow the accuracy gap between independent and collaborative inference modes. For instance, on the UTKFace dataset, X-VFL exhibits a tiny performance gap of less than 0.2% between independent inference (88.15%) and collaborative inference (88.32%). In contrast, baseline methods suffer a significant accuracy drop of over 20% when switching from collaborative to independent inference. A similar trend is observed across other datasets, indicating X-VFL’s robustness in maintaining consistent performance.

## 4.2 Results under varying overlap ratios of aligned data samples

To evaluate the effect of varying overlap ratios of aligned data samples, we test these methods with 20%, 40%, and 80% aligned samples, under a fixed feature missing rate of  $R_{\text{miss}} = 0.5$ . The performance results on CIFAR-10 and MIMIC-III are presented in Fig. 9a and Fig. 9b, respectively.

As illustrated, X-VFL consistently outperforms the baseline methods across all overlap ratios in both independent and collaborative inference modes. For instance, on the CIFAR-10 dataset (Fig. 9a), X-VFL achieves over 45% accuracy in the independent inference mode at a 40% overlap ratio, whereas the three baseline methods all fall below 35%. Similarly, in the collaborative inference mode, X-VFL attains over 65% accuracy at the same 40% overlap ratio, compared to around 55% for the baseline methods.

Also, a similar trend is observed on the MIMIC-III dataset (Fig. 9b), further demonstrating X-VFL’s robustness and superior performance, particularly under low overlap ratios.

## 4.3 Results under imbalanced training data across clients

To evaluate the impact of data imbalance between clients for these methods, we consider a 20% data imbalance setting, where client A and client B hold 80% and 20% of the total data, respectively, including both aligned and non-aligned samples. This setup enables a thorough evaluation of the impact of imbalanced training data on classification performance. The performance gap between the data-rich and data-poor clients also offers an interesting point of analysis. Experimental results for independent inference under a feature missing rate of  $R_{\text{miss}} = 0.5$  are presented in Fig. 10.

As demonstrated in Fig. 10, the baseline methods exhibit substantial performance gaps between the two clients, particularly on the MIMIC-III dataset, where the data-rich client A consistently outperforms the data-poor client B by 36.06%, 35.85%, and 36.29%. These gaps highlight the inability of baseline methods to effectively handle data imbalance, leading to significantly degraded performance for the data-poor client B. In contrast, our X-VFL substantially reduces this gap to just 8.42%, demonstrating its superior ability to balance the performance between data-rich and data-poor clients, by completing the missing features through the XCom module. A similar yet more compelling trend is observed on the CIFAR-10 dataset. While baseline methods fail to adequately support the data-poor client B, X-VFL not only narrows the performance gap but also slightly improves the accuracy of the data-poor client B. This unexpected gain can be attributed to the design of the XCom module, which leverages the richer data from client A to enhance the feature representations for the data-poor client B by reconstructing its missing features, thus improving classification performance despite the severe data imbalance.

## 5 Conclusion

In this paper, we proposed X-VFL, a novel VFL framework that addresses key challenges of conventional VFLs by effectively handling datasets with partially missing features and enabling locally independent inference at each client. In particular, X-VFL introduces two key modules: Cross Completion (XCom) and Decision Subspace Alignment (DS-Align). XCom is designed to complete missing features for non-aligned data samples by exploiting cross-client information, thereby effectively increasing the volume of data available for training and inference. DS-Align aligns local features with completed and global features across all clients within the decision subspace, enabling each client to perform locally independent inference, even in the presence of missing features. In addition, theoretical convergence theorems are established for different algorithms used in training X-VFL. Extensive experiments on real-world datasets demonstrate that X-VFL significantly outperforms existing VFL methods, validating its practical effectiveness and superiority in addressing key challenges such as missing features, locally independent inference, and data imbalance.

## Acknowledgments

This research was supported by the Singapore Ministry of Education (MOE) Academic Research Fund (AcRF) Tier 1 grant.

## References

Timothy Castiglia, Shiqiang Wang, and Stacy Patterson. Self-supervised vertical federated learning. In *Workshop on Federated Learning: Recent Advances and New Challenges, in Conjunction with*

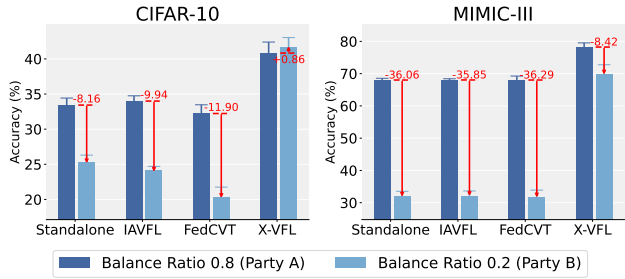


Figure 10: Performance comparison under data imbalance on the CIFAR-10 and MIMIC-III datasets.

*NeurIPS 2022*, 2022a.

- Timothy J Castiglia, Anirban Das, Shiqiang Wang, and Stacy Patterson. Compressed-VFL: Communication-efficient learning with vertically partitioned data. In *Proceedings of the 39th International Conference on Machine Learning*, pages 2738–2766. PMLR, 17–23 Jul 2022b.
- Jia Deng, Wei Dong, Richard Socher, Li-Jia Li, Kai Li, and Li Fei-Fei. ImageNet: A large-scale hierarchical image database. In *2009 IEEE Conference on Computer Vision and Pattern Recognition*, pages 248–255. IEEE Computer Society, 2009.
- Cong Fang, Chris Junchi Li, Zhouchen Lin, and Tong Zhang. Spider: Near-optimal non-convex optimization via stochastic path-integrated differential estimator. *Advances in neural information processing systems*, 31, 2018.
- Fangcheng Fu, Xupeng Miao, Jiawei Jiang, Huanran Xue, and Bin Cui. Towards communication-efficient vertical federated learning training via cache-enabled local updates. *Proceedings of the VLDB Endowment*, 15(10):2111–2120, June 2022.
- Saeed Ghadimi, Guanghui Lan, and Hongchao Zhang. Mini-batch stochastic approximation methods for nonconvex stochastic composite optimization. *Mathematical Programming*, 155(1):267–305, 2016.
- Chung-ju Huang, Leye Wang, and Xiao Han. Vertical federated knowledge transfer via representation distillation for healthcare collaboration networks. In *Proceedings of the ACM Web Conference 2023*, pages 4188–4199, 2023.
- Lingxiao Huang, Zhize Li, Jialin Sun, and Haoyu Zhao. Coresets for vertical federated learning: Regularized linear regression and  $K$ -means clustering. *Advances in Neural Information Processing Systems*, 35:29566–29581, 2022.
- Alistair EW Johnson, Tom J Pollard, Lu Shen, Li-wei H Lehman, Mengling Feng, Mohammad Ghassemi, Benjamin Moody, Peter Szolovits, Leo Anthony Celi, and Roger G Mark. Mimic-iii, a freely accessible critical care database. *Scientific data*, 3(1):1–9, 2016.
- Madhura Joshi, Ankit Pal, and Malaikannan Sankarasubbu. Federated learning for healthcare domain - pipeline, applications and challenges. *ACM Transactions on Computing for Healthcare*, 3(4), 2022.
- Peter Kairouz, H Brendan McMahan, Brendan Avent, Aurélien Bellet, Mehdi Benni, Arjun Nitin Bhagoji, Kallista Bonawitz, Zachary Charles, Graham Cormode, Rachel Cummings, et al. Advances and open problems in federated learning. *Foundations and Trends® in Machine Learning*, 14(1–2):1–210, 2021.
- Yan Kang, Yang Liu, and Xinle Liang. FedCVT: Semi-supervised vertical federated learning with cross-view training. *ACM Transactions on Intelligent Systems and Technology*, 13(4):1–16, 2022.
- Alex Krizhevsky, Geoffrey Hinton, et al. Learning multiple layers of features from tiny images. 2009.
- Wenjie Li, Qiaolin Xia, Hao Cheng, Kouyin Xue, and Shu-Tao Xia. Vertical semi-federated learning for efficient online advertising. *arXiv preprint arXiv:2209.15635*, 2022a.

Wenjie Li, Qiaolin Xia, Junfeng Deng, Hao Cheng, Jiangming Liu, Kouying Xue, Yong Cheng, and Shu-Tao Xia. VFed-SSD: Towards practical vertical federated advertising. *arXiv preprint arXiv:2205.15987*, 2022b.

Zhize Li and Peter Richtárik. A unified analysis of stochastic gradient methods for nonconvex federated optimization. *arXiv preprint arXiv:2006.07013*, 2020.

Zhize Li, Hongyan Bao, Xiangliang Zhang, and Peter Richtárik. PAGE: A simple and optimal probabilistic gradient estimator for nonconvex optimization. In *International conference on machine learning*, pages 6286–6295. PMLR, 2021.

Deron Liang, Chia-Chi Lu, Chih-Fong Tsai, and Guan-An Shih. Financial ratios and corporate governance indicators in bankruptcy prediction: A comprehensive study. *European Journal of Operational Research*, 252(2):561–572, 2016.

Tao Lin, Lingjing Kong, Sebastian U Stich, and Martin Jaggi. Ensemble distillation for robust model fusion in federated learning. *Advances in Neural Information Processing Systems*, 33: 2351–2363, 2020.

Yang Liu, Yan Kang, Tianyuan Zou, Yanhong Pu, Yuanqin He, Xiaozhou Ye, Ye Ouyang, Ya-Qin Zhang, and Qiang Yang. Vertical federated learning: Concepts, advances, and challenges. *IEEE Transactions on Knowledge and Data Engineering*, 2024.

H Brendan McMahan, Eider Moore, Daniel Ramage, Seth Hampson, and Blaise Agüera y Arcas. Communication-efficient learning of deep networks from decentralized data. In *International Conference on Artificial Intelligence and Statistics*, pages 1273–1282. PMLR, 2017.

Zhenghang Ren, Liu Yang, and Kai Chen. Improving availability of vertical federated learning: Relaxing inference on non-overlapping data. *ACM Transactions on Intelligent Systems and Technology*, 13(4):1–20, 2022.

Chandra Thapa, Pathum Chamikara Mahawaga Arachchige, Seyit Camtepe, and Lichao Sun. Splitfed: When federated learning meets split learning. In *Proceedings of the AAAI Conference on Artificial Intelligence*, volume 36, pages 8485–8493, 2022.

Pedro Valdeira, Shiqiang Wang, and Yuejie Chi. Vertical federated learning with missing features during training and inference. In *The Thirteenth International Conference on Learning Representations*, 2025.

Praneeth Vepakomma, Otkrist Gupta, Tristan Swedish, and Ramesh Raskar. Split learning for health: Distributed deep learning without sharing raw patient data. *arXiv preprint arXiv:1812.00564*, 2018.

Jian Xu, Xinyi Tong, and Shao-Lun Huang. Personalized federated learning with feature alignment and classifier collaboration. *arXiv preprint arXiv:2306.11867*, 2023.

Qiang Yang, Yang Liu, Tianjian Chen, and Yongxin Tong. Federated machine learning: Concept and applications. *ACM Transactions on Intelligent Systems and Technology*, 10(2):1–19, 2019.

Zhifei Zhang, Yang Song, and Hairong Qi. Age progression/regression by conditional adversarial autoencoder. In *IEEE Conference on Computer Vision and Pattern Recognition*, 2017.

## A Missing Proofs

In this appendix, we provide the detailed proofs for our convergence Theorems 1 and 2 in Appendix A.1 and Appendix A.2, respectively.

### A.1 Proof of Theorem 1

According to SGD-type update  $\boldsymbol{\theta}^{t+1} = \boldsymbol{\theta}^t - \eta \tilde{\nabla} L(\boldsymbol{\theta}^t)$  and the smoothness Assumption 1, we have

$$\mathbb{E}_t[L(\boldsymbol{\theta}^{t+1})] \leq \mathbb{E}_t[L(\boldsymbol{\theta}^t) + \langle \nabla L(\boldsymbol{\theta}^t), \boldsymbol{\theta}^{t+1} - \boldsymbol{\theta}^t \rangle + \frac{\beta}{2} \|\boldsymbol{\theta}^{t+1} - \boldsymbol{\theta}^t\|^2] \quad (12)$$

$$= \mathbb{E}_t[L(\boldsymbol{\theta}^t) - \eta \langle \nabla L(\boldsymbol{\theta}^t), \tilde{\nabla} L(\boldsymbol{\theta}^t) \rangle + \frac{\beta\eta^2}{2} \|\tilde{\nabla} L(\boldsymbol{\theta}^t)\|^2] \quad (13)$$

$$\leq L(\boldsymbol{\theta}^t) - (\eta - \frac{\beta\eta^2}{2}) \|\nabla L(\boldsymbol{\theta}^t)\|^2 + \frac{\beta\eta^2\sigma^2}{2}, \quad (14)$$

where  $\mathbb{E}_t$  takes the expectation conditioned on all history before step  $t$ , and Eq. (14) uses Assumption 2.

Summing up Eq. (14) from  $t = 0$  to  $T - 1$  and rearranging terms, we get

$$(\eta - \frac{\beta\eta^2}{2}) \sum_{t=0}^{T-1} \mathbb{E} \|\nabla L(\boldsymbol{\theta}^t)\|^2 \leq L(\boldsymbol{\theta}^0) - \mathbb{E}[L(\boldsymbol{\theta}^t)] + \frac{\beta\eta^2\sigma^2 T}{2} \quad (15)$$

$$\frac{1}{T} \sum_{t=0}^{T-1} \mathbb{E} \|\nabla L(\boldsymbol{\theta}^t)\|^2 \leq \frac{\Delta_0}{(\eta - \beta\eta^2/2)T} + \frac{\beta\eta^2\sigma^2}{2\eta - \beta\eta^2}, \quad (16)$$

where  $\Delta_0 := L(\boldsymbol{\theta}^0) - L^*$ . Note that  $\frac{\beta\eta^2\sigma^2}{2\eta - \beta\eta^2} \leq \frac{\Delta_0}{(\eta - \beta\eta^2/2)T}$  if  $\eta \leq \sqrt{\frac{2\Delta_0}{\beta\sigma^2 T}}$ . Thus it is not hard to obtain, by choosing the learning rate  $\eta \leq \min\{\frac{2}{\beta}, \sqrt{\frac{2\Delta_0}{\beta\sigma^2 T}}\}$ ,

$$\frac{1}{T} \sum_{t=0}^{T-1} \mathbb{E} \|\nabla L(\boldsymbol{\theta}^t)\|^2 \leq O\left(\sqrt{\frac{\beta\Delta_0\sigma^2}{T}}\right) = O\left(\frac{1}{\sqrt{T}}\right) = \epsilon^2. \quad (17)$$

This means that after  $T = O(\frac{1}{\epsilon^4})$  steps, SGD-type algorithms can find a suitable parameter  $\hat{\boldsymbol{\theta}}$  for X-VFL such that  $\mathbb{E} \|\nabla L(\hat{\boldsymbol{\theta}})\|^2 \leq \epsilon^2$ , where  $\epsilon$  denotes the convergence error.  $\square$

### A.2 Proof of Theorem 2

The variance in stochastic gradients leads to a large number of communication rounds (i.e., update steps  $T$ ). We now prove that the optimal variance-reduced PAGE-type method (Li et al., 2021) effectively reduces the variance and thus largely decreases the total number of communication rounds (Theorem 2).

According to simplified PAGE update step Eq. (10) and Lemma 4 of PAGE (Li et al., 2021), we have the following variance reduction lemma:

**Lemma 1** Suppose that Assumptions 1 and 2 hold. For the probabilistic gradient estimator  $\mathbf{g}^t$  defined in Eq. (10), we have

$$\mathbb{E}_t[\|\mathbf{g}^t - \nabla L(\boldsymbol{\theta}^t)\|^2] \leq (1-p)\|\mathbf{g}^{t-1} - \nabla L(\boldsymbol{\theta}^{t-1})\|^2 + \frac{(1-p)\beta^2}{b'} \|\boldsymbol{\theta}^t - \boldsymbol{\theta}^{t-1}\|^2 + \frac{p\sigma^2}{b}. \quad (18)$$

This lemma indicates that the variance is roughly reduced by a factor  $1 - p$  after each update step. Then according to the descent Lemma 2 of PAGE (Li et al., 2021), we have

$$L(\boldsymbol{\theta}^{t+1}) \leq L(\boldsymbol{\theta}^t) - \frac{\eta}{2} \|\nabla f(\boldsymbol{\theta}^t)\|^2 - \left(\frac{1}{2\eta} - \frac{\beta}{2}\right) \|\boldsymbol{\theta}^{t+1} - \boldsymbol{\theta}^t\|^2 + \frac{\eta}{2} \|\mathbf{g}^t - \nabla L(\boldsymbol{\theta}^t)\|^2. \quad (19)$$

Taking the expectation and combining Eq. (19) with multiple Eq. (18), we obtain

$$\begin{aligned} & \mathbb{E}[L(\boldsymbol{\theta}^{t+1}) - L^* + \frac{\eta}{2p} \|\mathbf{g}^{t+1} - \nabla L(\boldsymbol{\theta}^{t+1})\|^2] \\ & \leq \mathbb{E}\left[L(\boldsymbol{\theta}^t) - L^* - \frac{\eta}{2} \|\nabla L(\boldsymbol{\theta}^t)\|^2 - \left(\frac{1}{2\eta} - \frac{\beta}{2}\right) \|\boldsymbol{\theta}^{t+1} - \boldsymbol{\theta}^t\|^2 + \frac{\eta}{2} \|\mathbf{g}^t - \nabla L(\boldsymbol{\theta}^t)\|^2\right. \\ & \quad \left. + \frac{\eta}{2p} \left( (1-p) \|\mathbf{g}^t - \nabla L(\boldsymbol{\theta}^t)\|^2 + \frac{(1-p)\beta^2}{b'} \|\boldsymbol{\theta}^{t+1} - \boldsymbol{\theta}^t\|^2 + \frac{p\sigma^2}{b} \right) \right] \end{aligned} \quad (20)$$

$$\begin{aligned} & = \mathbb{E}\left[L(\boldsymbol{\theta}^t) - L^* + \frac{\eta}{2p} \|\mathbf{g}^t - \nabla L(\boldsymbol{\theta}^t)\|^2 - \frac{\eta}{2} \|\nabla L(\boldsymbol{\theta}^t)\|^2 + \frac{\eta\sigma^2}{2b}\right. \\ & \quad \left. - \left(\frac{1}{2\eta} - \frac{\beta}{2} - \frac{(1-p)\eta\beta^2}{2pb'}\right) \|\boldsymbol{\theta}^{t+1} - \boldsymbol{\theta}^t\|^2 \right] \end{aligned} \quad (21)$$

$$\leq \mathbb{E}\left[L(\boldsymbol{\theta}^t) - L^* + \frac{\eta}{2p} \|\mathbf{g}^t - \nabla L(\boldsymbol{\theta}^t)\|^2 - \frac{\eta}{2} \|\nabla L(\boldsymbol{\theta}^t)\|^2 + \frac{\eta\sigma^2}{2b}\right], \quad (22)$$

where Eq. (22) holds due to  $\frac{1}{2\eta} - \frac{\beta}{2} - \frac{(1-p)\eta\beta^2}{2pb'} \geq 0$  by choosing learning rate  $\eta \leq \frac{1}{\beta(1+\sqrt{(1-p)/(pb')})}$ .

Summing up Eq. (22) from  $t = 0$  to  $T - 1$  and rearranging terms, we get

$$\frac{\eta}{2} \sum_{t=0}^{T-1} \mathbb{E} \|\nabla L(\boldsymbol{\theta}^t)\|^2 \leq \mathbb{E}\left[L(\boldsymbol{\theta}^0) - L^* + \frac{\eta}{2p} \|\mathbf{g}^0 - \nabla L(\boldsymbol{\theta}^0)\|^2 + \frac{\eta\sigma^2 T}{2b}\right] \quad (23)$$

$$\frac{1}{T} \sum_{t=0}^{T-1} \mathbb{E} \|\nabla L(\boldsymbol{\theta}^t)\|^2 \leq \frac{2\Delta_0}{\eta T} + \frac{\sigma^2}{pbT} + \frac{\sigma^2}{b}, \quad (24)$$

where Eq. (24) uses  $\Delta_0 := L(\boldsymbol{\theta}^0) - L^*$  and the bounded variance Assumption 2 for the initial gradient estimator  $\mathbf{g}^0 = \tilde{\nabla}_b L(\boldsymbol{\theta}^0)$ .

Then for any convergence error  $\epsilon$ , by choosing learning rate  $\eta \leq \frac{1}{2\beta}$ , minibatch sizes  $b = \frac{2\sigma^2}{\epsilon^2}$ ,  $b' \leq \sqrt{b}$ , and probability  $p = \frac{b'}{b+b'}$ , we have

$$\frac{1}{T} \sum_{t=0}^{T-1} \mathbb{E} \|\nabla L(\boldsymbol{\theta}^t)\|^2 \leq O\left(\frac{1}{T}\right) = \epsilon^2. \quad (25)$$

This means that after  $T = O(\frac{1}{\epsilon^2})$  steps, PAGE-type algorithms can find a suitable parameter  $\hat{\boldsymbol{\theta}}$  for X-VFL such that  $\mathbb{E} \|\nabla L(\hat{\boldsymbol{\theta}})\|^2 \leq \epsilon^2$ , where  $\epsilon$  denotes the convergence error. Compared with the SGD-type algorithms in Theorem 1, the variace-reduced PAGE-type algorithms in Theorem 2 significantly decreases the total number of communication rounds, i.e., from  $T = O(\frac{1}{\epsilon^4})$  to  $T = O(\frac{1}{\epsilon^2})$  by a factor of  $\frac{1}{\epsilon^2}$ .  $\square$

## B Experimental Details

We now provide more details of the experimental setup in this appendix. We conduct the experiments on real-world datasets, including three image datasets: CIFAR-10 (Krizhevsky et al., 2009), TinyImageNet (restricted to five classes) (Deng et al., 2009), and UTKFace (Zhang et al., 2017), as well as three tabular datasets: MIMIC-III (Johnson et al., 2016), Bank (Liang et al., 2016), and Avazu (Kang et al., 2022). For the image datasets, features are vertically partitioned into disjoint subsets and assigned to different clients. For the tabular datasets, continuous features are normalized to the range  $[0, 1]$ , while categorical features are transformed into one-hot encodings (Bank) or embedding-based representations (Avazu). These preprocessed features are then partitioned into disjoint subsets and distributed to the clients. The server retains the class labels of the datasets.

To simulate real-world scenarios where clients have partially missing features, we mask a proportion of features in the non-aligned training and test samples. Various feature missing rates  $R_{\text{miss}} = \{0, 0.1, 0.3, 0.5, 0.7, 0.9, 1\}$  are applied to thoroughly assess the impact of missing features.

For the image datasets (CIFAR-10, TinyImageNet, and UTKFace), the client’s local (bottom) model is implemented using a residual network with varying depths, characterized by different numbers of residual blocks. The corresponding server (top) model is a six-layer fully connected neural network (FCNN). For the tabular datasets (MIMIC-III, Bank, and Avazu), both the client and server models are implemented as three-layer FCNNs. The input dimensions of the server models were set to 2048 for image datasets and 512 for tabular datasets to accommodate differences in feature complexity and representation requirements. The batch size is set to 50. The hyperparameters  $\lambda_1$  and  $\lambda_2$  defined in the overall loss function (see Eq. (5)) are selected from the ranges listed in Table 1.

Table 1: Hyperparameter ranges for  $\lambda_1$  and  $\lambda_2$

Dataset	$\lambda_1$	$\lambda_2$
CIFAR-10	$\{0.01, 0.02, 0.05, 0.1, 0.2, 0.5\}$	$\{1 \times 10^{-5}, 2 \times 10^{-5}, 5 \times 10^{-5}, 1 \times 10^{-4}, 2 \times 10^{-4}, 5 \times 10^{-4}\}$
TinyImageNet	$\{1, 2, 5, 10, 20\}$	$\{5 \times 10^{-4}, 1 \times 10^{-3}, 2 \times 10^{-3}, 5 \times 10^{-3}\}$
UTKFace	$\{1, 2, 5, 10, 20\}$	$\{5 \times 10^{-4}, 1 \times 10^{-3}, 2 \times 10^{-3}, 5 \times 10^{-3}\}$
MIMIC-III	$\{5 \times 10^{-4}, 1 \times 10^{-3}, 2 \times 10^{-3}, 5 \times 10^{-3}, 1 \times 10^{-2}\}$	$\{0.02, 0.05, 0.1\}$
Bank	$\{1 \times 10^{-4}, 2 \times 10^{-4}, 5 \times 10^{-4}, 1 \times 10^{-3}\}$	$\{5 \times 10^{-5}, 1 \times 10^{-4}, 2 \times 10^{-4}, 5 \times 10^{-4}\}$
Avazu	$\{1 \times 10^{-4}, 2 \times 10^{-4}, 5 \times 10^{-4}, 1 \times 10^{-3}\}$	$\{1 \times 10^{-5}, 2 \times 10^{-5}, 5 \times 10^{-5}, 1 \times 10^{-4}, 2 \times 10^{-4}\}$

Vanilla Standalone refers to an independently trained model in which each client uses only its own local features for training and inference. It serves as a baseline for evaluating the capability of independent inference. Vanilla VFL enables collaborative training by concatenating local feature representations from all clients at a central server. During inference, these concatenated representations are performed to generate predictions. This approach serves as a baseline for evaluating the capability of collaborative inference. For other baselines, although previous studies typically either cannot handle missing features or do not support locally independent inference, we identify two related works, IAVFL (Ren et al., 2022) and FedCVT (Kang et al., 2022), that are relevant for comparison, as discussed in Section 1.2. Concretely, we compare our X-VFL with these four baselines for both independent Inference and collaborative inference modes, using test classification accuracy as the performance metric. All results are averaged over five random seeds to ensure robustness.

## C Additional Experimental Results for TinyImageNet and Bank

Similar to Section 4.1, this appendix provides additional experimental results on the TinyImageNet and Bank datasets under varying feature missing rates. The results are presented in Fig. 11 and Fig. 12. Moreover, the results demonstrate the same trend: our X-VFL significantly outperforms the baselines, particularly in the independent inference mode—one of the key challenges that X-VFL is designed to address.

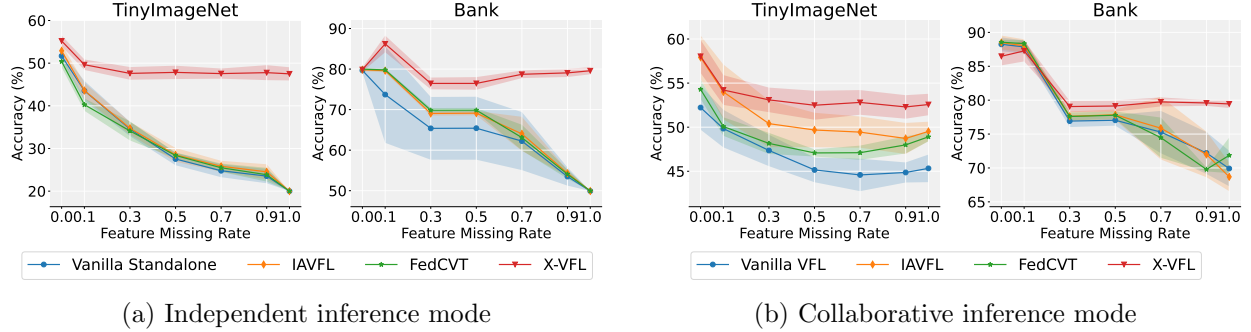


Figure 11: Performance comparison under varying feature missing rates on the TinyImagenet and Bank datasets.

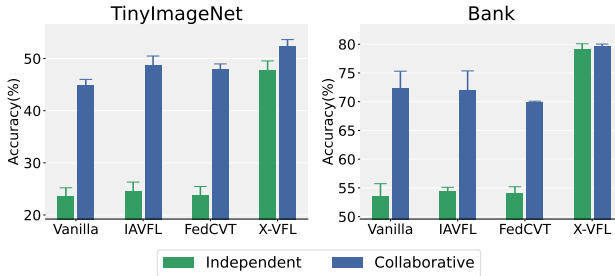


Figure 12: Performance difference between independent and collaborative inference modes under feature missing rate  $R_{\text{miss}} = 0.9$  on the TinyImagenet and Bank datasets.

## D General Multiple Clients Setting

In this appendix, we present the extension of our X-VFL framework to the general case with multiple  $k$  clients. This extension enhances the practicality of X-VFL and offers a more scalable and effective approach for broader applications. The framework formulation and corresponding experimental results are provided in Appendix D.1 and Appendix D.2, respectively.

### D.1 Formulation for multiple clients

Similar to Section 2.1, let  $f_1, \dots, f_k$  denote the local models for the  $k$  clients. Then  $\mathbf{E}_i = f_i(\mathbf{x}_i)$  denotes the feature embeddings/representations for client  $i$ ,  $i \in [k]$ . For the general case of  $k$  clients,

the overall loss function can be formulated as the same one as in Eq. (5):

$$L = L_{\text{decision}} + \lambda_1 L_{\text{DSAlign}_1} + \lambda_2 L_{\text{DSAlign}_2}. \quad (26)$$

Compared with two-client setting, now the classification decision loss for  $k$  clients is formulated as follows:

$$L_{\text{decision}} = \sum_{i \in \mathcal{M}} \ell(h(\mathbf{E}_i), y) + \ell(h(\frac{\mathbf{E}'}{m}), y) + \ell(h(\frac{\tilde{\mathbf{E}}' + \mathbf{E}'}{k}), y) + \sum_{i=1}^k \ell(h(\frac{\tilde{\mathbf{E}}_i + \mathbf{E}_{-i}}{k}), y), \quad (27)$$

where  $\mathbf{E}' = \sum_{j \in \mathcal{M}} \mathbf{E}_j$ ,  $\tilde{\mathbf{E}}' = \sum_{i \in \{1, \dots, k\} \setminus \mathcal{M}} \tilde{\mathbf{E}}'_i$ ,  $\mathcal{M} \subseteq \{1, \dots, k\}$  denotes the subset of clients that hold full local features (i.e., clients without missing features), where  $|\mathcal{M}| = m$  for some  $m \leq k$ ,  $\mathbf{E}_{-i} = \sum_{j \in \{1, \dots, k\} \setminus \{i\}} \mathbf{E}_j$ , and

$$\tilde{\mathbf{E}}_i = f_i(\tilde{\mathbf{X}}_i), \quad \tilde{\mathbf{X}}_i = \text{XCom}_i(\frac{\mathbf{E}_{-i}}{k-1}), \quad 1 \leq i \leq k, \quad (28)$$

$$\tilde{\mathbf{E}}'_i = f_i(\tilde{\mathbf{X}}'_i), \quad \tilde{\mathbf{X}}'_i = \text{XCom}_i(\frac{\mathbf{E}'}{m}), \quad 1 \leq i \leq k. \quad (29)$$

For aligned data, the following terms in Eq. (27) are activated:  $\sum_{i \in \mathcal{M}} \ell(h(\mathbf{E}_i), y)$ ,  $\ell(h(\frac{\mathbf{E}'}{m}), y)$ , and  $\sum_{i=1}^k \ell(h(\frac{\tilde{\mathbf{E}}_i + \mathbf{E}_{-i}}{k}), y)$ . The term  $\ell(h(\frac{\tilde{\mathbf{E}}' + \mathbf{E}'}{k}), y)$  is not activated, as  $\tilde{\mathbf{E}}'$  is empty when  $\mathcal{M}$  includes all clients (i.e.,  $k = m$ ). For non-aligned data, the activated terms are  $\sum_{i \in \mathcal{M}} \ell(h(\mathbf{E}_i), y)$ ,  $\ell(h(\frac{\mathbf{E}'}{m}), y)$ , and  $\ell(h(\frac{\tilde{\mathbf{E}}' + \mathbf{E}'}{k}), y)$ .

The last two loss components introduced by our DS-Align module in the general case of  $k$  clients are formulated as follows:

$$L_{\text{DSAlign}_1} = \sum_{i=1}^k \ell(h(\tilde{\mathbf{E}}_i), h(\mathbf{E}_i)), \quad (30)$$

and

$$L_{\text{DSAlign}_2} = \sum_{i=1}^k \ell(h(\mathbf{E}_i), h(\frac{\sum_{i=1}^k \mathbf{E}_i}{k})). \quad (31)$$

## D.2 Experimental results for multiple clients

In this appendix, we provide the experimental results for the general multiple clients setting. We use CIFAR-10 (Krizhevsky et al., 2009) as the image dataset and MIMIC-III (Johnson et al., 2016) as the tabular dataset. In particular, we conduct experiments with  $k = 4$  clients. Regarding the baselines, since FedCVT (Kang et al., 2022) is specifically designed for the two-client scenario, it cannot be extended to the multi-client setting. Therefore, we include three baseline methods (Vanilla Standalone, Vanilla VFL, IAVFL) in the multi-client experiments, consistent with those used in the two-client setting, excluding only FedCVT. The implementation details remain the same as in the two-client case (see Appendix B), except that the batch size is set to 100. In the multi-client setting, we simply set the hyperparameters  $\lambda_1 = \lambda_2 = 0.01$ .

Fig. 13 presents the results under varying feature missing rates,  $R_{\text{miss}} = \{0, 0.3, 0.5, 0.7, 1.0\}$ , for both independent and collaborative inference modes. A comparison of performance between these two modes at a missing rate  $R_{\text{miss}} = 0.7$  is shown in Fig. 14. The results follow the same

trend observed in the two-client case: our X-VFL significantly outperforms the baselines, particularly in the independent inference mode—one of the key challenges that X-VFL is designed to address. Moreover, Fig. 14 highlights the advantage of X-VFL in effectively narrowing the accuracy gap between independent and collaborative inference modes.

We also evaluate the effect of varying overlap ratios of aligned data samples, using 20%, 40%, and 80% aligned samples, as shown in Fig. 15. Similar to the two-client case, X-VFL consistently outperforms the baseline methods across all overlap ratios in both independent and collaborative inference modes.

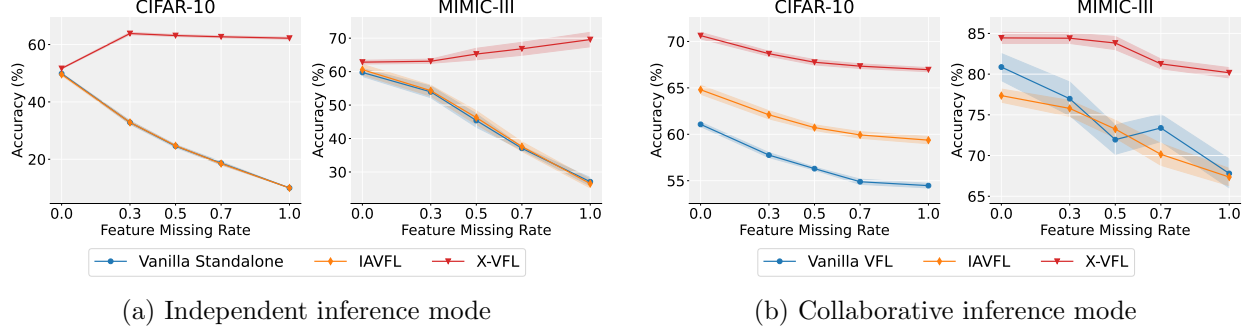


Figure 13: Performance comparison under varying feature missing rates on the CIFAR-10 and MIMIC-III datasets in the multiple clients setting.

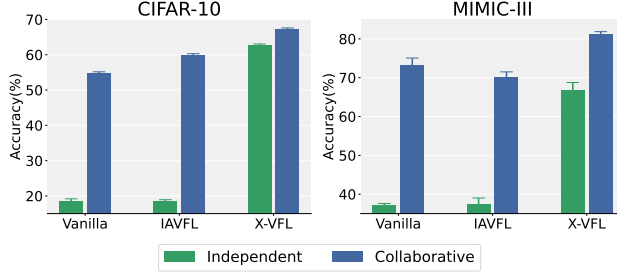


Figure 14: Performance comparison between independent and collaborative inference modes under feature missing rate of 0.7 on the CIFAR-10 and MIMIC-III datasets in the multiple clients setting.

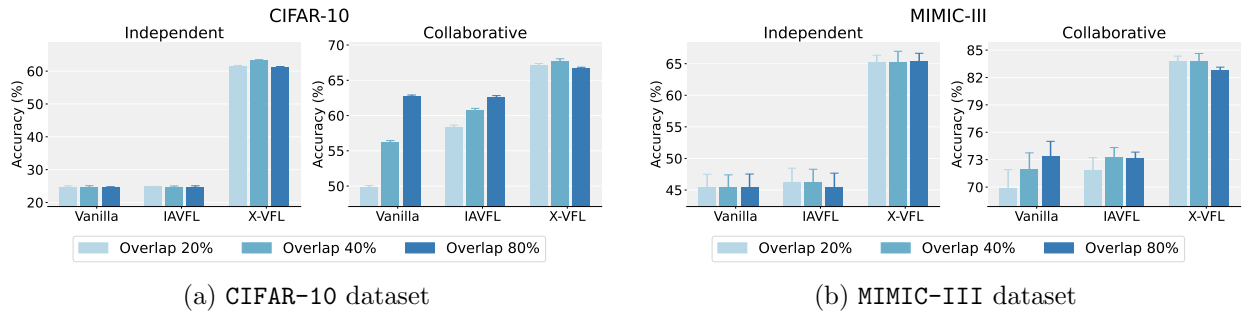


Figure 15: Performance comparison under varying overlap ratios on the CIFAR-10 and MIMIC-III datasets in the multiple clients setting.